

GA-A27301

CONCEPTUAL DESIGN OF THE TANGENTIAL INTERFEROMETER POLARIMETER DENSITY MEASUREMENTS

by

M.A. VAN ZEELAND, R.L. BOIVIN, D.L. BROWER, T.N. CARLSTROM, J.A. CHAVEZ,
W.X. DING, R. FEDER, D. JOHNSON, L. LIN, R.C. O'NEILL, and C. WATTS

JULY 2012



DISCLAIMER

This report was prepared as an account of work sponsored by an agency of the United States Government. Neither the United States Government nor any agency thereof, nor any of their employees, makes any warranty, express or implied, or assumes any legal liability or responsibility for the accuracy, completeness, or usefulness of any information, apparatus, product, or process disclosed, or represents that its use would not infringe privately owned rights. Reference herein to any specific commercial product, process, or service by trade name, trademark, manufacturer, or otherwise, does not necessarily constitute or imply its endorsement, recommendation, or favoring by the United States Government or any agency thereof. The views and opinions of authors expressed herein do not necessarily state or reflect those of the United States Government or any agency thereof.

CONCEPTUAL DESIGN OF THE TANGENTIAL INTERFEROMETER POLARIMETER DENSITY MEASUREMENTS

by

M.A. VAN ZEELAND, R.L. BOIVIN, D.L. BROWER,* T.N. CARLSTROM, J.A. CHAVEZ,
W.X. DING,* R. FEDER,† D. JOHNSON,† L. LIN,* R.C. O'NEILL, and C. WATTS‡

This is a preprint of a paper to be presented at the Nineteenth High Temperature Plasma Diagnostics Conference, May 6-10, 2012 in Monterey, California and to be submitted for publication in *Rev. Sci. Instrum.*

*University of California Los Angeles, Los Angeles, California.

†Princeton Plasma Physics Laboratory, Princeton, New Jersey.

‡ITER Organization, Cedex, France.

Work supported in part by
the General Atomics IR&D Funding and
the U.S. Department of Energy
under DE-FG02-08ER54984 and DE-AC02-09CH11466

GENERAL ATOMICS PROJECT 49008
JULY 2012



Conceptual Design of the Tangentially Viewing Combined Interferometer-Polarimeter for ITER Density Measurements^{a)}

M. A. Van Zeeland,^{1, b)} R. L. Boivin,¹ D. L. Brower,² T. N. Carlstrom,¹ J. A. Chavez,¹ W. X. Ding,² R. Feder,³ D. Johnson,³ L. Lin,² R. C. O'Neill,¹ and C. Watts⁴

¹⁾ General Atomics, P.O. Box 85608 San Diego, California 92186-5608, USA

²⁾ University of California-Los Angeles, Los Angeles, California, USA

³⁾ Princeton Plasma Physics Laboratory, P.O. Box 451, Princeton, New Jersey 08543, USA

⁴⁾ ITER Organization, 13115 St Paul Lez Durance, Cedex, France

(Dated: 20 July 2012)

One of the systems planned for the measurement of electron density in ITER is a multi-channel tangentially viewing combined interferometer-polarimeter (TIP). This work discusses the current status of the design, including a preliminary optical table layout, calibration options, error sources, and performance projections based on a CO₂/CO laser system. In the current design, two-color interferometry is carried out at 10.59 μm and 5.42 μm , and a separate polarimetry measurement of the plasma induced Faraday effect, utilizing the rotating wave technique, is made at 10.59 μm . The inclusion of polarimetry provides an independent measure of the electron density and can also be used to correct the conventional two-color interferometer for fringe skips at all densities, up to and beyond the Greenwald limit. The system features five chords with independent first mirrors to reduce risks associated with deposition, erosion, etc., and a common first wall hole to minimize penetration sizes. Simulations of performance for a projected ITER baseline discharge show the diagnostic will function as well as, or better than, comparable existing systems for feedback density control. Calculations also show that finite temperature effects will be significant in ITER even for moderate temperature plasmas and can lead to a significant underestimate of electron density.

PACS numbers: 52.70.Kz, 52.55.Fa, 52.25.Os, 52.70.m, 07.60.Ly, 07.60.Fs

I. INTRODUCTION

The primary system planned for real-time density control in ITER is the combined tangential interferometer and polarimeter (TIP).¹ TIP will also contribute to density profile reconstruction and play a secondary role as a diagnostic of core density fluctuations including those from broadband turbulence, MHD, and coherent modes such as Alfvén eigenmodes.^{2,3}

Initial conceptual design studies of the TIP were carried out in 1998⁴ and form the basis for the current design described here. This design uses a vibration compensated interferometer [two-color interferometer (TCI)]⁵⁻⁸ with a CO₂ laser at 10.59 μm for the probe beam and a CO laser at 5.42 μm for the vibration compensation.⁹ While this technique alone is well-established and used for feedback control on several tokamaks around the world, it does suffer from susceptibility to fringe-skip errors since the measured phase shifts are much larger than 2π . To guarantee continuous density control, the CO₂ probe beam is also used in a polarimeter configuration for measuring the density dependent plasma induced Faraday rotation.¹⁰⁻¹³ The rationale behind adding a polarimetry measurement to standard TCI is that for the majority of operating

conditions the expected Faraday rotation of 10.59 μm radiation will always be less than 2π , making fringe skips irrelevant. This additional measurement can then be used for renormalizing TCI measurements, should a fringe skip occur, or as an independent measure of line-integrated density¹⁰ and possibly for feedback density control by itself.

Both interferometers and the polarimeter described here measure a phase shift. What is ultimately desired, however, is information about the plasma density evolution. The phase shift for each wavelength interferometer can be expressed as¹⁴

$$\phi_i = A\lambda_i + 2\pi V/\lambda_i \quad , \quad (1)$$

where the first term ($A\lambda_i$) is the plasma contribution with A related to the line-integrated electron density (n_e) according to:

$$A = r_e \int n_e \left(1 - \frac{3T_e}{2m_e c^2} \right) dL \quad , \quad (2)$$

$r_e = 2.82 \times 10^{-15}$ m (the classical electron radius), m_e the electron mass and T_e the electron temperature. The second term ($2\pi V/\lambda_i$) is the phase shift due to vibration (V) in the direction of beam propagation. Relativistic corrections are taken from Ref. 15. For a two-color interferometer, the line-integrated density including relativistic

^{a)} Contributed paper published as part of the Proceedings of the 19th Topical Conference on High-Temperature Plasma Diagnostics, Monterey, California, May 2012.

^{b)} Electronic mail: vanzeeland@fusion.gat.com.

tic effects is given by

$$\int n_e \left(1 - \frac{3T_e}{2m_e c^2} \right) dL = \frac{\lambda_{co2}}{r_e (\lambda_{co2}^2 - \lambda_{co}^2)} \times \left[\phi_{co2} - \phi_{co} \frac{\lambda_{co}}{\lambda_{co2}} \right], \quad (3)$$

where for the current ITER design using CO and CO₂ lasers, $\lambda_{co} = 5.42 \mu\text{m}$ and $\lambda_{co2} = 10.59 \mu\text{m}$. Similarly, the magnetic field weighted density integral measured by the polarimeter is given by

$$\int n_e \left(1 - \frac{2T_e}{m_e c^2} \right) \vec{B} \cdot d\vec{L} = \frac{\alpha}{C_p \lambda_{co2}^2}, \quad (4)$$

where α is the Faraday rotation angle (the actual measured polarimeter phase shift is 2α), B is the local magnetic field, and $C_p = 2.62 \times 10^{-13}$ rad/T. Equations (3) and (4) represent the actual physical quantities obtainable from the instruments themselves with no additional information from any other diagnostic or calculation. The primary source of error on the interferometer density integral in Eq. (3) is due to phase measurement errors (typically 1-5 deg) and likewise for the polarimeter (typically 0.01-0.1 deg). Secondary errors for the interferometer measurement can result from inaccurate determination of the wavelength ratio (10^{-4} error in $\lambda_{co}/\lambda_{co2}$ with $V = 2$ mm causes equivalent of 5 deg phase error) and for the polarimeter from the finite frequency difference of the RH and LH rotating waves described in the next section ($V = 2$ mm causes equivalent of 0.012 deg phase error for 4 MHz frequency difference) — both errors become significant with increased vibration V .

II. TIP TABLE LAYOUT AND DETECTION

An initial design of the optical table component layout for an individual TIP chord has been developed and is shown in Fig. 1. Each chord fits entirely on a single 5×7 ft optical table and uses several off-the-shelf components or standard components with custom optical coatings (components listed in figure caption).

The basic principle of operation is that radiation from a single $10.59 \mu\text{m}$ CO₂ laser (frequency $\omega_0 = 2.8 \times 10^{13}$ Hz) is used to create both RH and LH circularly polarized radiation (Plasma Leg) with a difference frequency of $\delta\omega = (\omega_2 - \omega_1)$, (where $\omega_1 = 38$ MHz and $\omega_2 = 42$ MHz) as well as horizontally polarized light with frequency ω_o (Reference Leg). Combined, the RH and LH beams form a linearly polarized wave with its plane of polarization rotating at $\delta\omega/2$. As described below, this allows a phase measurement to be made for determination of both the interferometric phase shift and Faraday rotation, analogous to techniques developed using FIR lasers on RTP,^{16,17} and MST.^{18,19} This composite beam is split (BS4) and a fraction is used to form the optical Local Oscillator (LO). After being combined with a fraction of the reference leg power at frequency ω_o , the

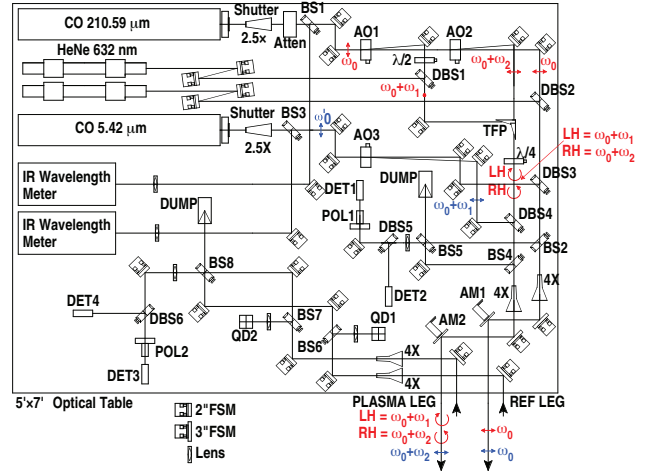


FIG. 1. Optical table layout of individual TIP chord. Red/blue labels show CO₂/CO laser radiation frequencies and polarization. HeNe lasers are for alignment purposes only. Component description: 2.5X = 2.5X beam expander (1 CO₂ and 1 CO), *Atten* = 50 W capable attenuator, *BS1, BS3, BS6, BS7* = ZnSe beamsplitter (45 deg AOI, $R \approx 5\%/T \approx 95\%$, at 5.42 and 10.59 μm), *AO1, AO2, AO3* = Germanium Acousto-Optic Modulator 38-42 MHz capable, $\lambda/2$ = CdS half-wave plate, *DBS1, DBS2* = ZnSe beam combiner (45 deg AOI, $R \approx 99\%$ at 632 nm/ $T \approx 99\%$ at 10.59 μm), *TFP* = ZnSe thin film polarizer, $\lambda/4 = 10.59 \mu\text{m}$ CdS quarter-wave plate, *DBS3, DBS4, DBS5, DBS6* = beam combiner (45 deg AOI, $R \approx 99\%$ at 5.42 μm and $T \approx 99\%$ at 10.59 μm and 632 nm), *BS2, BS4* = ZnSe beamsplitter (45 deg AOI, $R \approx 10\%/T \approx 90\%$ at 5.42, 10.59 μm and 632 nm), *BS5, BS8* = ZnSe beamsplitter (45 deg AOI, $R \approx 50\%/T \approx 50\%$ at 5.42, 10.59 μm and 632 nm), *DET1, DET2, DET3, DET4* = HgCdTe PV detectors, *Pol1, Pol2* = 10.59 μm ZnSe Brewster Angle Based Polarizer, *AM1, AM2* = active piezo electric mirror mount, *4X* = 4X broadband reflective optic beam expander, *QD1, QD2* = HgCdTe quadrant detectors, *FSM* = front surface mirrors.

combined beams are sent through a polarizer and to a reference detector (Detector 1). Detector 1 signals at frequencies $(\omega_2 - \omega_1)$ and ω_1 are essentially used to form the LO waveforms for demodulation of the Faraday rotation and interferometry phase shifts respectively. The majority of the RH and LH beams are sent through the ITER plasma and back (Plasma Leg), then through a polarizer and to a separate detector (Detector 3) after being combined again with a separate reference leg that is approximately the same path length (Ref Leg).

Detector 1 sees an intensity signal given by

$$I_1(t) \approx A_{112} \sin[(\omega_2 - \omega_1)t + \phi_{v12}(t)] + A_{11} \sin[\omega_1 t + \phi_{v1}(t)] + A_{12} \sin[\omega_2 t + \phi_{v2}(t)] \quad (5)$$

and Detector 3 sees

$$I_3(t) \approx A_{312} \sin[(\omega_2 - \omega_1)t + \phi_{v12}(t) + 2\alpha(t)] + A_{31} \sin[\omega_1 t + \phi_{v1}(t) + \phi_1(t)] + A_{32} \sin[\omega_2 t + \phi_{v2}(t) + \phi_2(t)]. \quad (6)$$

Therefore, heterodyne detection at frequency ($\omega_2 - \omega_1$) can be applied to determine the Faraday rotation (α) where the LO signal is $I1(t)$ and the IF signal is $I3(t)$. Similarly, the interferometric phase shift of the CO₂ beam, $\phi_1(t)$, can be obtained through heterodyne detection at frequency ω_1 , where again the LO signal is $I1(t)$ and the IF signal is $I3(t)$. As discussed in previous sections, the interferometric phase shift, $\phi_1(t)$, that is observed at Detector 3 contains contributions from both vibration and the plasma. The same process could also be carried out at ω_2 , however, the small variation in frequency $\omega_1/\omega_0 \approx \omega_2/\omega_0 \ll 1$ may make this unnecessary. Separation of the plasma and vibration induced phase shifts, is accomplished by using a second co-linear CO laser based interferometer operating at $5.42 \mu\text{m}$ where the LO signal is taken at ω_1 from Detector 2 and the IF signal is from Detector 4 — so called vibration compensated two-color interferometry.

The formation of the separate frequency RH and LH CO₂ laser radiation is accomplished by acousto-optic (AO) frequency shifters functioning at ω_1 and ω_2 respectively. The drive for the AO cells is adjusted such that the incident beam is split into approximately equal amplitude components at ω_0 , $\omega_0 + \omega_1$, and $\omega_0 + \omega_2$ with linear polarization in the plane of the paper. The $\omega_0 + \omega_1$ component is then passed through a CdS $\lambda/2$ waveplate and its polarization is rotated by 90 deg. The two separate frequencies ($\omega_0 + \omega_1$, and $\omega_0 + \omega_2$), orthogonally polarized beams are then re-combined using a ZnSe thin film polarizer/combiner (TFP) operating at Brewster's angle. The composite beam is then passed through a CdS $\lambda/4$ waveplate with its axis at 45 deg with respect the polarization vector of each frequency component forming the superimposed counter-rotating LH and RH waves at $\omega_0 + \omega_1$, and $\omega_0 + \omega_2$ respectively (i.e. rotating linearly polarized wave).

Wavelength monitoring, which is important for obtaining accurate vibration compensation in the presence of large motion, is accomplished in real-time via two IR wavelength meters. It is noted that the wavelength measured is the unshifted wavelength while the slightly shifted wavelength is what is actually probing the plasma. Alternatively, these signals could be taken from either of the dumped beam fractions following beamsplitter BS5 or BS8 in Fig. 1. The difference being that all three frequencies would be present for the CO₂ ($\omega_0, \omega_0 + \omega_1$, and $\omega_0 + \omega_2$) and both for the CO ($\omega_0, \omega_0 + \omega_1$).

Not shown in Fig. 1 is a half-wave plate that will be inserted periodically after the quarter-wave plate. This wave plate will be used to calibrate the polarimeter and account for any ellipticity as well as component coatings that may occur.^{12,20} Alternatively, if real-time calibration of the polarimeter is required, a photo-elastic-modulator (PEM) may replace or be inserted in addition to the half-wave plate.

Some of the components used for the feedback alignment system are also present on the TIP optical table. Active mirrors AM1 and AM2 are piezo-electric mirror

mounts controlled by quadrant detectors near the port plug. These function to keep the reference and plasma legs at the same position on their respective quadrant detector (not shown). The quadrant detectors QD1 and QD2 are used to provide position feedback to a separate set of piezo electric mirror mounts positioned off the optical table. The plasma leg active mirror near the port plug is shown in Fig. 2. The mirrors are adjusted such that the reference and plasma leg positions on QD1 and QD2 respectively are held constant. It is noted that an additional active mirror may be required to maintain interference signal on the final beamsplitter in the presence of large plasma leg motion.

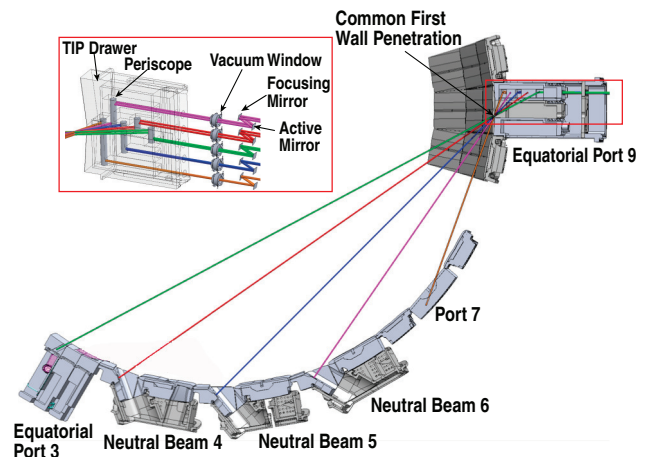


FIG. 2. CATIA model of TIP layout on ITER. The 5 TIP chords enter ITER through equatorial port 9.

III. TIP LAYOUT ON ITER

The TIP system features five chords with independent first mirrors to reduce risks associated with deposition and erosion as well as a common first wall hole to minimize penetration sizes. Each of the five beams are delivered to ITER using free-space optics. The beams enter the vessel through equatorial port 9 and are returned parallel with a finite-offset resulting from reflection off a retroreflector. Each of the beams will have a final focusing mirror near the port plug followed by an active mirror controlled by the quadrant detectors labelled QD2 in Fig. 1. The return beams are oriented as to arrange for a vertical offset in the actual plasma. Averaging occurs in the offset direction, so a vertical offset as opposed to horizontal was chosen since that is the elongated plasma direction and the local parallel magnetic field is relatively constant in that direction. Three of the retroreflectors are located in neutral beam heating blankets and two in other equatorial ports. Roundtrip path lengths range from 108-124 m and Gaussian beam modeling show for the innermost chord, the $10.59 \mu\text{m}$ beam $1/e^2$ radius is $<12 \text{ mm}$

over the entire path and the $5.42\ \mu\text{m}$ beam radius is $<11\ \text{mm}$ over the entire path. Beam radii at the retro-reflectors are $7.83\ \text{mm}\ \text{CO}_2/3.92\ \text{mm}\ \text{CO}$ and $3.4\ \text{mm}\ \text{CO}_2/2.1\ \text{mm}\ \text{CO}$ for the innermost and outermost tangency radii respectively. The vessel windows are envisioned to be either CVD diamond or potentially BaF_2 , pending analysis. Both windows fulfill two basic necessities, a low Verdet constant at $10.59\ \mu\text{m}^{21,22}$ (to avoid contamination of Faraday rotation measurements) and acceptable transmission at both $10.59\ \mu\text{m}$ and $5.42\ \mu\text{m}$. Additionally, both materials have the added benefit of similar indices of refraction at $10.59\ \mu\text{m}$ and $5.42\ \mu\text{m}$ (<http://www.luxpop.com/RefractiveIndexList.html>), reducing uncompensated optical path differences due to perpendicular displacements.

IV. PERFORMANCE PROJECTIONS

To simulate the performance of the TIP system during plasma current rampup, flattop, and rampdown, a DINA simulation of a representative 15 MA scenario was used to obtain the necessary discharge information. This scenario has the plasma current rampup during 70 s, start of burn at 90 s, end of burn at 500 s.²³ The relevant discharge parameters are shown in Fig. 3. Since no information is given on the actual density profile, a flat profile is assumed inside of the LCFS. The interferometer and polarimeter phase shifts are calculated assuming a $10.59\ \mu\text{m}$ probing wavelength. Figure 3(a) and 3(b) shows the temporal evolution of the LCFS shape and plasma current combined with electron density in the time range $t = 0.1 - 100\ \text{s}$. This time window corresponds to the current rampup and flattop and continues until density flattop is achieved. Also overlaid on Fig. 3(a) are the tangency radii of the various chords. TIP simulation results for this time range are shown in Fig. 3(c) and 3(d), where the interferometer phase shifts and measured polarimeter phase change due to Faraday rotation are given. The colors correspond to the various tangency radii shown in Fig. 3(a). Twice the Faraday rotation angle is given for the polarimeter because that is the measurable phase shift. It can be seen from Fig. 3(a,b) that the maximum measured interferometer phase shift corresponds to roughly ten full fringes while the measured Faraday rotation angle is always less than a full fringe, eliminating any possible phase ambiguity. In fact, the polarimeter measured phase shift is always less than π even for densities up to the Greenwald density of approximately $1.2 \times 10^{20}\ \text{m}^{-3}$. Thus, in the event of a fringe skip in the interferometer system, one would be able to re-normalize using the polarimeter.

Figure 4 shows the relative errors for both the interferometer ($\delta nL/nL$) and polarimeter ($\delta nBL/nBL$) corresponding to the assumed conservative fixed instrumental errors of $\delta\phi = 10$ degrees and $\delta\alpha = 0.1$ degrees for the interferometer and polarimeter respectively. For the in-

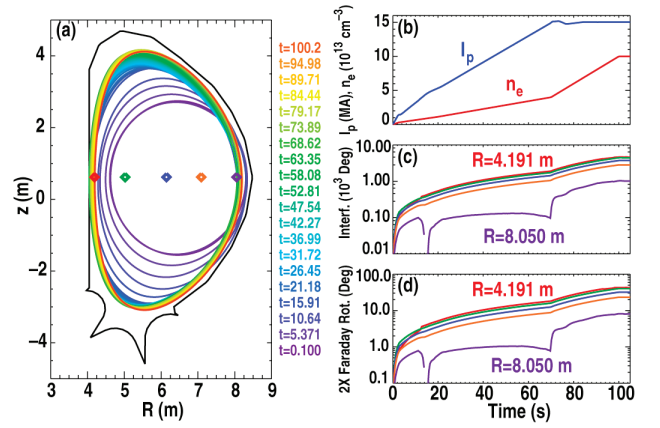


FIG. 3. (a) Shape of LCFS during current rampup. Tangency radii of the five TIP chords overlaid as colored diamonds (red = 4.191 m, green = 5.021 m, blue = 6.145 m, orange = 7.090 m, purple = 8.050 m). (b) Plasma current and electron density vs time. (c) Measured interferometer phase shift for the five tangency radii vs time. (d) Measured phase shift due to Faraday rotation vs time for the five tangency radii.

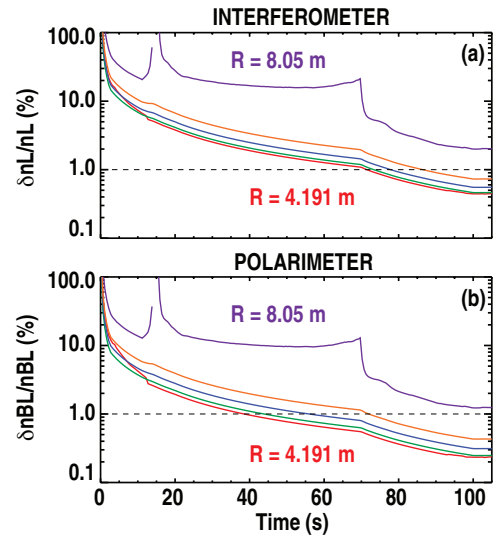


FIG. 4. Relative error for (a) interferometer and (b) polarimeter measurements during the current rampup time window shown in Fig. 3. Each tangency radius is represented by a color corresponding to that in Fig. 3.

terferometer, nL represents the line-integrated density given by Eq. (3) and for the polarimeter, nBL represents the magnetic field weight density integral given by Eq. (4). Overlaid in each figure is the nominal target accuracy of 1% as specified in Table 2 of Ref. 1 (note, the 1% specification in Ref. 1) was on line-averaged density which would also include path length errors). According to Fig. 4, both the interferometer and polarimeter would be capable of fulfilling this requirement with all but one chord by approximately 90 s (flattop). Due to retro-reflector placement restrictions, the outermost chord is at very large radius and actually misses the plasma briefly

near $t = 18$ s. This chord, however, will be a very useful constraint on edge density profiles since it traverses only large minor radii where edge gradients are largest.

Because the plasma starts from zero density, it is obviously impossible to satisfy 1% relative accuracy at all times. With respect to plasma control during startup, 1% relative error may not be necessary. To help put these TIP simulations in context, a database search of all DIII-D discharges from 2008-2010 was carried out in which density and current ramp information were retrieved. In these discharges, a CO₂/HeNe (10.59 μm /0.6328 μm) two color interferometer was used for density control.²⁴ These data show that adequate density control during the current ramp on DIII-D is obtained with 10% relative error at 40% of peak current and relative errors at the beginning of flattop above 2%. The measurement error is larger than the average plasma induced phase shift until approximately 10% peak current. These data point to the fact that, with regard to error levels, the ITER TIP system should function as well as, or better than, that on DIII-D for feedback control during current rampup. Additionally, it is pointed out that the ITER error estimates used are very conservative, in fact, the same database search for DIII-D showed a typical resolution of 3-5 degrees (with <1 deg possible¹⁴) and polarimeter measurements with 0.01 deg resolution have been made on other devices.¹¹

V. FINITE TEMPERATURE EFFECTS

As the equations for the interferometer phase shift and Faraday rotation angle in the first section show, finite electron temperature can have a significant effect on the measurement. The magnitude of this effect for a flat density profile is shown in Fig. 5. As the plasma gets hotter, for a given density profile, the interferometer phase shift and Faraday rotation angle decrease – causing an underestimate of the line-averaged density. The highest predicted electron temperatures in ITER are in the ~ 40 keV range (the plasma in Fig. 3 is 10 keV) and electron temperature profiles are expected to be centrally peaked for all scenarios implying an average of approximately 20 keV. From Fig. 5, one can easily see this effect will be in the 5%-8% range for the interferometer and polarimeter respectively at the highest expected temperatures and, even for lower temperatures, will cause a significant systematic error in estimates of line-integrated density if a cold-plasma approximation is used. To meet ITER density specifications for line-averaged electron density measurements, finite electron temperature effects will have to be accounted for by both the interferometer and polarimeter. One approach to doing this is using the equations in the first section to obtain the effect itself. By assuming an average $B_{||}$, the interferometer and polarimeter temperature dependent density correction fac-

tor can be written as:

$$\int n_e \frac{T_e}{m_e c^2} dL = \frac{2\lambda_{co2}}{r_e(\lambda_{co2}^2 - \lambda_{co}^2)} \times \left[\phi_{co2} - \phi_{co} \frac{\lambda_{co}}{\lambda_{co2}} \right] - \frac{2\alpha}{B_{||} C_p \lambda_{co2}^2} \quad (7)$$

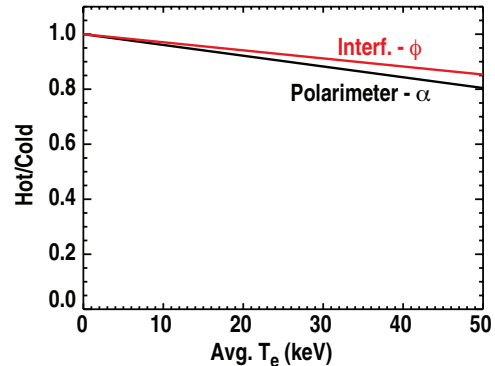


FIG. 5. Effect of finite temperature on the measured interferometer phase shift (ϕ) and Faraday rotation angle (α) - plotted as ratio of finite temperature shift or rotation over that for a cold plasma.

This allows the relativistic factors to be backed out and the impact on the density measurements removed while simultaneously enjoying the benefit of additional information about the average electron temperature.

VI. SUMMARY

The current status of the conceptual design for the ITER tangential interferometer/polarimeter (TIP) has been presented. The design uses two-color interferometry at 10.59 μm and 5.42 μm , and a separate polarimetry measurement of the plasma induced Faraday rotation at 10.59 μm . The inclusion of polarimetry allows the two-color system to recover unambiguously from fringe skips at all densities, up to and beyond the Greenwald limit as well as the ability to use the polarimeter itself for feedback density control. The system features five chords with independent first mirrors and a common first wall hole to minimize penetration sizes. Simulations of performance for a projected ITER baseline discharge show the diagnostic will meet ITER requirements and function as well as, or better than, comparable existing systems for feedback density control. Calculations also show that finite temperature effects will be significant in ITER even for moderate temperature plasmas and can lead to an underestimate of electron density.

ACKNOWLEDGMENTS

This work was supported in part by the General Atomics IR&D funds and the US Department of Energy under DE-FG02-08ER54984 and DE-AC02-09CH11466.

- ¹A. J. H. Donne, *et al.*, Nucl. Fusion **47**, S337 (2007).
- ²M. A. Van Zeeland and G. J. Kramer, "Measurements of Alfvén Eigenmodes in Fusion Plasmas," AIP Conf. Proc. **988**, 103 (2008).
- ³M. A. Van Zeeland, *et al.*, Plasma Phys. Controlled Fusion **47**, L31 (2005).
- ⁴T. N. Carlstrom, *et al.*, "Baseline Design of a Multi-channel Interferometer and Polarimeter System for Density Measurements on ITER," Diagnostics for Experimental Thermonuclear Fusion Reactors 2, Edited by Stott *et al.*, Plenum Press, New York (1998).
- ⁵D. R. Baker and S. T. Lee, Rev. Sci. Instrum. **49**, 919 (1978).
- ⁶T. Lehecka, W. A. Peebles, C. Luhmann, and T. N. Carlstrom, Rev. Sci. Instrum. **8**, 1580 (1988).
- ⁷J. Irby, *et al.*, Rev. Sci. Instrum. **59**, 1568 (1988).
- ⁸Yasunori Kawano, *et al.*, Rev. Sci. Instrum. **67**, 1520 (1996).
- ⁹P. Innocente, *et al.*, Rev. Sci. Instrum. **68**, 694 (1997).
- ¹⁰Y. Kawano, S. Chiba, H. Shirai, A. Inoue, and A. Nagashima, Rev. Sci. Instrum. **70**, 1430 (1999).
- ¹¹T. Akiyama, *et al.*, Rev. Sci. Instrum. **72**, 1073 (2001).
- ¹²T. Kondoh, *et al.*, Rev. Sci. Instrum. **75**, 3420 (2004).
- ¹³M. A. Van Zeeland, *et al.*, Rev. Sci. Instrum. **79**, 10E719 (2008).
- ¹⁴M. A. Van Zeeland, R. L. Boivin, T. N. Carlstrom, T. Deterly, D. K. Finkenthal, Rev. Sci. Instrum. **77**, 10F325-1 (2006).
- ¹⁵V. V. Mirnov, *et al.*, Phys. Plasmas **14**, 102105 (2007).
- ¹⁶J. H. Rommers and J. Howard Plasma Phys. Controlled Fusion **38**, 1805 (1996).
- ¹⁷J. H. Rommers, A. J. H. Donne, F. A. Karelse, and J. Howard Rev. Sci. Instrum. **68**, 1217 (1997).
- ¹⁸D. L. Brower, *et al.*, Rev. Sci. Instrum. **72**, 1077 (2001).
- ¹⁹W. X. Ding, *et al.*, Rev. Sci. Instrum. **75**, 3387 (2004).
- ²⁰D.L. Brower, *et al.*, Rev. Sci. Instrum. **74**, 1534 (2003).
- ²¹Yasunori Kawano, Shinichi Chib, and Akira Inoue, Rev. Sci. Instrum. **75**, 279 (2004).
- ²²M. H. Kim, V. Kurz, G. Acbas, C. T. Ellis, J. Cerne, JOSA B **28**, 199 (2011).
- ²³DINA simulation, ITER_D.2KTYCQ, (2009).
- ²⁴T. N. Carlstrom, D. R. Ahlgren, and J. Crosbie, Rev. Sci. Instrum. **7**, 1063 (1988).